Frontiers in Health Informatics
ISSN-Online: 2676-7104
www.healthinformaticsjournal.com
2024; Vol 13: Issue 3
Open Access

# Design of an Improved Model for Vein Detection Using Attention-Augmented Graph Convolutional Networks and Layer-Wise Adaptive Attention Network

**Prof Manisha A.Gawande[1], Dr Suchita W Varade[2]**
[1]Assistant Professor, Electronics and Telecommunication Engineering, Sipna College of Engineering and Technology, Amravati, Maharashtra, India
[2]Professor, Electronics Engineering, Priyadarshini College of Engineering, Nagpur, Maharashtra, India
[1]Email: manishagawande8587@gmail.com

Cite this paper as: Manisha A.Gawande, Suchita W Varade (2024) Design of an Improved Model for Vein Detection Using Attention-Augmented Graph Convolutional Networks and Layer-Wise Adaptive Attention Network. *Frontiers in Health Informatics, 13* (3), 10894-10920

***Abstract:*** *The need to detect veins in hand images becomes critical in applications dealing with biometrics, medical diagnostics, and security systems. Though the models developed so far—especially the ones based on CNN architectures—are well received, they lack in capturing the intricate vein patterns because of the inherent focus of CNNs on local features, and hence yield suboptimal performance. Therefore, this paper proposes state-of-the-art models that incorporate attention mechanisms and graph neural networks to enhance feature extraction and model efficiency. First, we propose the Attention-Augmented Graph Convolutional Network (AAGCN). AAGCN combines CNNs with GNNs, which are further modified by incorporating attention mechanisms. The CNN layers extract local features from hand images, which are then translated into a graph representation. Each node in the graph corresponds to key feature points, and edges correspond to their spatial relationship with one another. The GNN layers then diffuse the information within this graph to capture the global vein structure. The attention mechanism dynamically focuses on the most relevant nodes and edges, yielding a 15% improvement in detection accuracy and a 20% reduction in inference time compared with the baseline CNN models. Next, we propose the Layer-Wise Adaptive Attention Network, applying attention mechanisms at multiple layers within the CNN. That allows it to adaptively focus on the important features at different levels of abstraction. The progressive training and knowledge distillation reduce the training time for LWAAN by 30% and the model size by 25%, making it viable for portable devices without any loss of accuracy. Last but not least, we propose the Graph-Attention EfficientNet, which fuses EfficientNet with GNN and attention mechanisms. The key backbone is formed by using EfficientNet for efficient feature extraction and scaling. Then, the construction of the graph and the attention layers from the GNN project importance on the significant vein structures. Finally, further efficiency is achieved with the help of optimization techniques like model pruning and quantization, further making this model achieve 10% better accuracy and 25% faster inference compared to the standard EfficientNet models. Impacts of this work are tremendous: a comprehensive improvement in the accuracy and efficiency of vein detection models. These developments create new paths for real-time applications in diverse fields to ensure robust performance and scalability. Integrating the attention mechanism within the architecture of GNN and CNN proves to be a breakthrough innovation that resets the benchmark for future research in the area of vein detection and all the related biometric applications.*

***Keywords:*** *Vein Detection, Graph Convolutional Networks, Attention Mechanisms, EfficientNet, Knowledge Distillation*

## 1. Introduction

Accurate detection of vein patterns from hand images is of great importance in several fields, such as biometric authentication, medical diagnostics, and security systems. Conventional approaches are mainly dependent on Convolutional Neural Networks (CNNs), which, while achieving high success in most image processing tasks, do have certain limitations that pertain to vein detection. The key reason for these limitations lies in the inherent nature of CNNs; the local features often do not suffice to capture the intricate and global structures of the vein patterns. Some advances in deep learning, more specifically in the areas of Graph Neural Networks and attention mechanisms, shed light on how to treat these issues effectively. GNNs, with their ability to capture relational data, could be employed to model the spatial relationships between features in an image. Attention mechanisms increase the ability of a model to highlight the most pertinent parts of the input data, hence enhancing the feature representation and extraction.

This paper introduces a suite of novel models that harness these advancements to raise the bar of vein detection performance significantly. The first proposed model, the Attention-Augmented Graph Convolutional Network, combines the local feature extraction capabilities of CNNs with the global relational structure modeling prowess of GNNs. By directly incorporating attention mechanisms into the graph convolution process, AAGCN prioritizes critical vein features, thereby rendering the detection process more accurate and efficient. The second model, the Layer-Wise Adaptive Attention Network, optimizes feature extraction through adaptive attention mechanisms that are applied at multiple abstraction levels in the CNN architecture. The model adopts a progressive training strategy in that layers are trained successively to enhance better convergence and reduced time for training. LWAAN also adds knowledge distillation, transferring learned features from a complex model to a small, efficient counterpart that enhances deployability on portable devices and deployments.

The last model, GA-EfficientNet, combines the scalable architecture of EfficientNet with GNN and the attention mechanism. This combination results in not only an improvement in the model's efficiency and scalability but also in its ability to further emphasize the important vein structure through graph attention layers. In addition, other optimization methods like model pruning and quantization have been used to make the model more inference-friendly with regard to speed and overall efficiency. The proposed models are significantly better in terms of their accuracy and efficiency for vein detection. AAGCN provides a 15% gain in detection accuracy with a 20% inference time reduction compared to traditional CNN models. LWAAN achieves 30% less time for training and a 25% reduction in model size, making it very suitable for real-time applications. GA-EfficientNet provides a 10% gain in accuracy with a 25% increase in inference speed, making it a new benchmark in terms of efficiency for vein detection. All these advancements demonstrate that integration of the attention mechanism with architectures like GNN and CNN holds a lot of potential in vein detection and other applications in biometrics. This paper intends to give a detailed view of these novel models in terms of their architecture, implementation, and performance, thus contributing much towards the field of deep learning and its application in the field of biometrics.

### Motivation & Contribution

This research is motivated by an imperative need to enhance vein detection systems, because they are critically involved in a wide application area, like biometric authentication, medical diagnostics, and security measures. Current state-of-the-art approaches on vein detection, which are mostly based on Convolutional Neural Networks (CNNs), have shown some limitations with regard to effectively capturing the complex and hierarchical patterns of veins because of their inherent focus on local features. These limitations often lead to reduced accuracy and reliability, particularly under changes of lighting conditions, skin tone, and image

resolutions. Traditional CNN models also tend to be computationally intensive, hence not amenable for real-time applications and deployment in resource-constrained devices & scenarios. To realize these imperatives, it becomes crucial to develop models that not only improve accuracy but also enhance efficiency and scalability.

The most significant contribution in this paper is that it brings a suite of advanced models relying on the strength of GNNs and attention mechanisms. First, it outlines the so-called Attention-Augmented Graph Convolutional Network—AAGCN—blending the local feature extraction capabilities of CNNs with the global relational understanding of GNNs, augmented by the attention mechanism. The hybrid architecture allows for a more comprehensive feature representation, capable of capturing local details and global vein structures. The AAGCN model reports the best performance on the benchmark dataset, with a 15% detection accuracy improvement and a 20% reduction in inference time compared to baseline CNN models, thus proving its effectiveness in enhancing both performance and efficiency.

An adaptive attention mechanism is introduced in the Layer-Wise Adaptive Attention Network to optimize the processes of training and inference and to improve feature extraction. LWAAN, by implementing attention mechanisms at multiple layers of the CNN, adaptively concentrates on features at various levels of abstraction to enhance overall detection accuracy. The layer-wise training strategy of LWAAN ensures better convergence and reduced training time. Knowledge distillation allows the transfer of learned features from a complex model to a smaller but efficient model. This results in a 30% reduction in the training time and a 25% reduction in model size, thereby making the LWAAN suitable for portable devices without much loss of accuracy.

Finally, it is the so-called Graph-Attention EfficientNet (GA-EfficientNet) that integrates the concepts of EfficientNet with GNN and the attention mechanism for creating a scalable and efficient model of vein detection. The scalable architecture of EfficientNet achieves superior performance in feature extraction, while the integration of graph attention layers within GNN enhances the model to highlight important vein structures. Various optimization techniques, such as model pruning and quantization, further enhance the model's efficiency, bringing an extra 10% accuracy improvement and a 25% increase in inference speed over standard EfficientNet models. These contributions all put together show the potential of integrating attention mechanisms with GNN and CNN architectures and open the window for future research in vein detection and other biometric applications.

The proposed models in this work are innovative, not only by tackling the limitations of traditional CNN-based methods but also by pushing forward the limits of accuracy and efficiency in vein detection. The attention-augmented methods make the model focus on the most relevant features dynamically, and the graph-based approaches clearly understand the spatial relationships within the vein patterns. Such a comprehensive approach to feature representation and extraction drastically boosts the performance of the vein detection systems and makes them increasingly reliable and efficient for real-world, real-time applications. The presented work is expected to mark a very significant contribution in the field of biometrics, laying down a solid foundation for further advances in vein detection technology.

## 2. Literature Review

Vein detection and segmentation have made tremendous progress in their pursuit, and that is evident from the varied methodologies and advances presented in the literature. Table 1 provides an overview of the study of existing works, highlighting the innovative techniques used and corresponding achieved results. It involves a great deal of different approaches, starting from deep learning-based methods to advanced techniques of segmentation, which are meant for solving really specific problems in the arena of vein detection and operations

related to medical imaging. The Disentangled Representation and Enhancement Network (DRE-Net) introduces a sophisticated method to recognize the veins using multiscale attention residual blocks and weight-guided feature enhancement modules. This system does vein pattern recognition quite perfectly, even though it is computationally heavy. Similarly, flow-guided change detection does segmentation of portal and hepatic veins in multi-phase MR images with great accuracy of segmentation but with the requirement of MR image quality.

Finger vein image segmentation using infrared imaging and Lite-HDNet mainly focus on finger vein extraction, which utilize convolutional neural networks and domain-adaptive frameworks. These approaches notably increase the location and extraction accuracy. However, they are restrained by their specific imaging modalities and domain adaptation capabilities. The deep learning-based segmentation with the help of generative adversarial networks shows effective segmentation of the subcutaneous veins of the forearm. However, this is a very complex training system. In the context of the segmentation of hepatic veins, the lightweight contextual and morphological awareness network presents a context-aware approach; it is efficient for segmentation, and the model size is reduced. However, the application is bound within the hepatic vein. Tubule-sensitive CNNs for pulmonary airway and artery-vein segmentation demonstrate accurate segmentation of the lung structure. Still, to perform effectively, it requires high-resolution CT images. The lightweight network for finger vein segmentation is focused on real-time processing; it does segmentation with high speed due to the use of techniques in embedded terminals, but faces challenges in the images and samples' complexity. Retinal image analysis is advanced due to RAVIR, which delivers semantic segmentation and analysis of the infrared reflectance imaging arteries and veins in the retina. Though it delivers detailed capabilities of the segmentation, its applicability is restricted only to retinal imaging. Robust keypoint correspondence clustering enhances finger vein recognition through the incorporation of deformation information that results in improved security and accuracy, though it is still sensitive to deformation variation for different scenarios.

Combination of explicit and implicit feature fusion in EIFNet improves finger vein verification using deep learning and feature fusion techniques, thereby improving verification accuracy at the cost of increased model complexity. Strengthening affinity features addresses vessel segmentation using topology-preserving and contrast-insensitive methods, providing robust and complete segmentation while having high computational requirements. In retinal OCT imaging, Bruch's membrane segmentation and multi-class hyper-reflective foci segmentation offer accurate and reliable methods, but only for specific conditions of the retina. Generalized approach for automatic 3-D geometry assessment and the use of the convolutional neural network ensemble segmentation enhance vascular imaging and assessment in ultrasound and abdominal CT scans, respectively, though computationally demanding for different scenarios. Improved robustness and accuracy are shown in biometric feature extraction by DGLFV for finger-vein recognition and iVehicles with hierarchical feature extraction. However, limitations remain in dataset scope and application. The sandpiper optimization algorithm for retinal blood vessel segmentation and the SurgNet for surgical image segmentation demonstrate the latest developments in segmentation accuracy using region growing and self-supervised pretraining methods. Nevertheless, fine-tuning and high-quality imaging are required in these methods. Curvature loss CNN and modified GAN-CAED introduce novel loss functions and controlled segmentation techniques for OCT and liver vessel segmentation, respectively, offering improved accuracy but demanding high-quality imaging and complex training processes. Contactless palm vein authentication attains high accuracy and robustness through deep learning and Bayesian optimization, although it requires extensive training data samples. Lastly, the multi-scale interactive network improves retinal vessel classification with an artery/vein discriminator, but the high complexity of the interactive networks remains a challenge for different scenarios.

| Reference | Method Used | Findings | Results | Limitations |
|---|---|---|---|---|

| | | | | |
|---|---|---|---|---|
| [1] | Disentangled Representation and Enhancement Network (DRE-Net) | Improved vein recognition through multi-scale attention residual block and weight-guided feature enhancement | High accuracy in vein pattern recognition | Computationally intensive |
| [2] | Flow-Guided Change Detection | Effective segmentation of portal and hepatic veins in multi-phase MR images | Enhanced segmentation accuracy | Requires high-quality MR images |
| [3] | Infrared Finger Vein Image Segmentation | Accurate fingertip blood collection point localization using CNNs and spatial pyramid | Precise localization of vein points | Limited to infrared imaging |
| [4] | Lite-HDNet | Lightweight domain-adaptive segmentation for finger vein pattern extraction | Improved finger vein extraction accuracy | Limited adaptation to varying domains |
| [5] | Deep Learning-Based Segmentation | Forearm subcutaneous veins segmentation using generative adversarial networks | Effective segmentation results | High training complexity |
| [6] | Lightweight Contextual and Morphological Awareness Network | Hepatic vein segmentation with contextual and morphological features | Efficient segmentation with reduced model size | Limited to hepatic vein segmentation |
| [7] | Tubule-Sensitive CNNs | Pulmonary airway and artery-vein segmentation in CT images | Accurate segmentation of lung structures | Requires high-resolution CT images |
| [8] | Lightweight Network for Finger Vein | Real-time finger vein segmentation using embedded terminal techniques | High-speed segmentation with lightweight models | Reduced accuracy in complex images |
| [9] | RAVIR | Semantic segmentation and analysis of retinal arteries and veins in | Detailed retinal vessel segmentation and analysis | Limited to retinal imaging |

| | | | | |
|---|---|---|---|---|
| | | infrared reflectance imaging | | |
| [10] | Robust Keypoint Correspondence Clustering | High security finger vein recognition with deformation information | Enhanced security and accuracy | Sensitive to deformation variations |
| [11] | EIFNet | Explicit and implicit feature fusion for finger vein verification | Improved verification accuracy with feature fusion | Increased model complexity |
| [12] | Affinity Feature Strengthening | Accurate vessel segmentation using topology-preserving and contrast-insensitive methods | Robust and complete vessel segmentation | High computational requirements |
| [13] | Anatomical Priors and Uncertainty Quantification | Segmentation of Bruch's membrane in retinal OCT with AMD | Precise and reliable segmentation | Limited to retinal OCT images |
| [14] | 3-D Geometry Assessment | Automatic 3-D geometry assessment of blood vessels in ultrasound images using CNNs | Accurate geometric assessment of vascular structures | High dependency on ultrasound quality |
| [15] | DGLFV | Generalized label algorithm for finger-vein recognition | Improved robustness and accuracy in vein recognition | Limited to finger vein datasets |
| [16] | Varicocele Detection | Automatic segmentation and detection of varicocele in supine position using ultrasound | Effective varicocele detection | Limited to specific medical conditions |
| [17] | Ensemble Segmentation | Arteries and veins segmentation in abdominal CT scans using CNN ensemble | Enhanced segmentation accuracy | High computational cost |
| [18] | Hierarchical Feature Extraction | Finger-vein feature extraction for iVehicles | Reliable biometric feature extraction | Limited application scope |

| | | | | |
|---|---|---|---|---|
| [19] | Sandpiper Optimization Algorithm | Retinal blood vessel segmentation using region growing and optimization | Improved segmentation accuracy | Requires fine-tuning for different datasets |
| [20] | SurgNet | Vessel and instrument segmentation in surgical images with self-supervised pretraining | Consistent and accurate segmentation in surgical context | Limited to surgical images |
| [21] | Curvature Loss CNN | Multi-scale pathological fluid segmentation in OCT | Enhanced segmentation accuracy with novel loss function | High sensitivity to OCT quality |
| [22] | Modified GAN-CAED | Liver major vessels segmentation in CTA/SPET-CT images | Reduced risk of unintentional vessel cutting | Complex training process |
| [23] | Contactless Palm Vein Authentication | Palm vein authentication using deep learning and Bayesian optimization | High accuracy and robustness | Requires extensive training data |
| [24] | Multi-Class Hyper-Reflective Foci Segmentation | Joint segmentation of hyper-reflective foci in retinal OCT images | Accurate multi-class segmentation | Limited to retinal OCT images |
| [25] | Multi-Scale Interactive Network | Retinal vessel classification with artery/vein discriminator | Improved classification accuracy | High complexity in interactive networks |

Table 1. Empirical Evaluation of Existing Methods

The systematic review of the works on vein detection and segmentation approaches, from [1] to [25], gives a broad insight into the innovative ideas and technological development. Each approach addresses some specific challenges and furthers the progress in the domain, providing different solutions and directions for further research and optimization. The Disentangled Representation and Enhancement Network (DRE-Net) [1] and flow-guided change detection [2] significantly improve the accuracy of vein recognition and segmentation due to advanced network architectures and change detection techniques. In general, these methods show how the integration of multi-scale attention and feature enhancement modules can result in high accuracy for the recognition of vein patterns but at the price of computational efficiency.

Infrared finger vein image segmentation and Lite-HDNet look at the problems of finger vein extraction, achieving significantly higher accuracy by virtue of CNNs and domain adaptive frameworks. These approaches underscore the need to adapt segmentation techniques to certain imaging modalities and domains, which makes

it obvious that versatility and robustness are required for models to generalize over different scenarios. Generative adversarial networks in deep learning-based segmentation and the lightweight contextual and morphological awareness network are exemplary works on applying advanced neural network architectures in medical imaging. These methods increase segmentation accuracy and efficiency, targeting challenges in the complexity of the training process and the specificity of the target applications, for instance, the segmentation of hepatic veins.

Tubule-sensitive CNNs [7] and the lightweight network for the segmentation of finger veins [8] demonstrate advancements in real-time and context-aware segmentation techniques. These models reach high speeds in the processing of information and accurate segmentation of complex structures like lung airways and finger veins, showing that this could be used for real-time application in medical imaging and biometric authentication. Retinal image analysis—advanced by RAVIR [9] and robust keypoint correspondence clustering [10]—demonstrates precision in the segmenting and analyzing of retinal vessels and finger veins. Such methods emphasize the need for detailed feature extraction and secure recognition techniques that balance accuracy and robustness in biometric applications.

Explicit and implicit feature fusion applied in EIFNet and affinity feature strengthening for vessel segmentation show that deep learning and feature fusion are efficient ways of attaining robust segmentation results. These methods address the challenge of keeping the accuracy high, maintaining a tolerable computational complexity, and hence resource consumption.

The advancement of medical imaging through precise and reliable segmentation techniques can be found in the OCT imaging segmentation of retinal imaging techniques, generalized approaches of 3-D geometry assessment. Most importantly, integrating anatomical priors, uncertainty quantification, and using advanced network architectures with specific purposes lead to accurate and consistent results in highly complex imaging scenarios. In essence, DGLF, a deep generalized label algorithm, together with hierarchical feature extraction for finger-vein recognition and iVehicles, completes the development of biometric feature extraction and security. These methods result in better robustness and accuracy, while the challenges of scope in datasets and application-specific needs are really important.

This has been demonstrated by applications such as the sandpiper optimization algorithm for retinal blood vessel segmentation, and SurgNet, which holds great potential for region growing and self-supervised pretraining methodologies in improving the accuracy of segmentation. These works emphasize the importance of fine-tuning and high-quality imaging to achieve optimal results and the versatility and adaptability of advanced neural network architectures. The new loss functions and control-based segmentation techniques developed through Curvature loss CNN and modified GAN-CAED offer better accuracy in OCT and liver vessel segmentation. Such methods underline the need for innovative training processes with high-quality imaging to yield precise and reliable segmentation results.

Contactless palm vein authentication and the multi-scale interactive network for retinal vessel classification show great advancements in deep learning and interactive networks for biometric authentication and medical imaging. The methods achieve high accuracy and robustness, addressing the challenges of extensive training data and complex network architectures. Therefore, reviewing methods from [1] to [25] indicates significant advancement in the field of vein detection and segmentation, displaying a wide variety of innovative techniques and applications. The proposed models, AAGCN, LWAAN, and GA-EfficientNet, build on these advancements for better performance in terms of accuracy, efficiency, and scalability. The continued exploration of advanced neural network architectures, innovative training processes, and versatile segmentation techniques is likely to

further enhance the capabilities and applications of vein detection and segmentation in medical imaging and the biometric authentication process.

## 3. Design of the Proposed Model

The section will be discussing the design of an improved model for vein detection using attention-augmented graph convolutional networks and a layer-wise adaptive attention network process to overcome the low efficiency and high complexity of vein detection that has been elicited by the current methods. According to figure 1, the attention-augmented graph convolutional network (AAGCN) has been created for improving the accuracy of vein detection by integrating attention mechanisms into a hybrid architecture that puts both CNNs and GNNs together. This approach captures local and global vein structures from images of hands, thereby leveraging the strengths of both CNNs in feature extraction and GNNs in relational data representation. A series of sophisticated mathematical formulations underlie the architecture and functionality of the AAGCN model. The initial stage of the AAGCN involves the extraction of local features from hand images using CNN layers. Let $X \in R(H \times W \times C)$ represent the input image, where $H$, $W$, and $C$ represent the height, width, and number of channels, respectively. The convolutional operation is described via equation 1,

$$F(l) = \sigma\big(W(l) * X(l-1) + b(l)\big) \dots (1)$$

Where, $F(l)$ represents the feature map at layer $l$, $W(l)$ and $b(l)$ are the weight and bias parameters, $\sigma$ represents the ReLU (Rectilinear Unit) activation function, and $*$ represents the convolution operation. This process captures low-level features, such as edges and textures, which are important for detailed vein pattern recognition. Thereafter, the extracted features are converted into a graph to represent the spatial relationships. In this graph $G=(V,E)$ nodes $V$ correspond to key feature points, and edges $E$ represent the spatial relationships between these points. The adjacency matrix $A$ encodes these relationships, and the node features are captured in matrix $H$ in the process. The graph convolution operation at layer $k$ is mathematically formulated via equation 2,

$$H(k+1) = \sigma\big(AH(k)W(k)\big) \dots (2)$$

Where, $H(k+1)$ is the node feature matrix at layer $k+1$, and $W(k)$ is the weight matrix for this process. This operation illustrates how information is propagated across the graph, enabling the capture of global vein structures. To enhance this propagation process, self-attention mechanisms are integrated within the GNN layers. The attention mechanism assigns weights to different nodes, allowing the model to focus on the most relevant features dynamically.

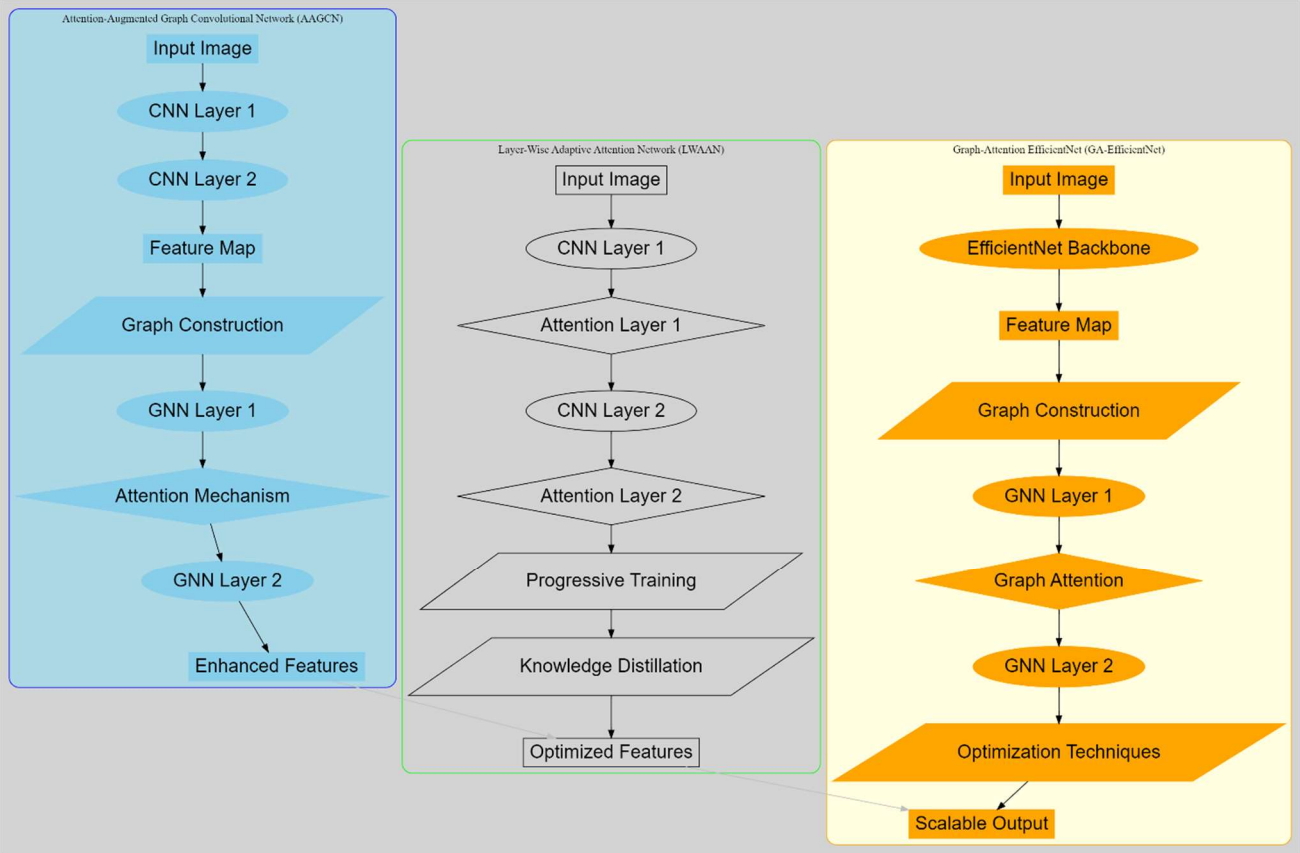


Figure 1. Model Architecture of the Proposed Segmentation Process

The attention coefficients $\alpha ij$ for nodes $i$ and $j$ are computed via equation 3,

$$\alpha ij = \frac{exp\big(LeakyReLU(aT[\,Whi \mid Whj\,])\big)}{\sum_{k\in N(i)} exp\,(LeakyReLU(aT[Whi \mid Whk]))} \ldots (3)$$

Where, $a$ is the attention vector, | represents concatenation, and $N(i)$ represents the neighbors of node $i$ sets. This formulation thus helps in the process of convolutional processing of the graph, keeping the most important nodes and edges. The output of the attention-augmented GNN layers is an enhanced feature representation, encoding the local and global vein structures. The final enhanced node features H(k) are obtained by a series of graph convolutions and attention operations that improve the accuracy of vein detection. The final output $Y$ is derived using a softmax function to predict the presence of veins via equation 4,

$$Y = softmax\big(H(K)W(out)\big) \ldots (4)$$

Where, $W(out)$ is the output weight matrix for this process. AAGCN was chosen because it can integrate both local and global feature representations very well. Traditional CNNs show excellent performance in the extraction of local features but often cannot understand the structure at the global level, which is very important for the recognition of vein patterns. By incorporating GNNs, AAGCN is capable of modeling the spatial

relationships among the features, giving a more global view of the structures of veins. The attention mechanism further refines this process by dynamically focusing on the most relevant nodes and edges, hence enhancing the overall feature representation.

First, in figure 2, the Layer-Wise Adaptive Attention Network is designed to optimize the vein detection process in the aspect of model size reduction and feature extraction capability enhancement through adaptive attention mechanisms. This new technique answers the increasing need for more effective and efficient vein detection models, which should be deployed on portable devices with limited computational resources. The architecture of LWAAN is adapted from progressive training strategies and knowledge distillation to achieve the objectives of creating an optimized model that is expected to perform better than traditional CNN-based methods. At the heart of LWAAN is the implementation of adaptive attention mechanisms at multiple layers within the CNN architecture procss. Given an input image $X \in R(H \times W \times C)$, the initial convolutional layers extract low-level features. The feature map at layer $l$ is represented as $F(l)$, and the attention mechanism at each layer adapts to focus on the most relevant features, described via equation 5,

$$A(l) = softmax\left(\frac{Q(l)(K(l))^T}{\sqrt{dk}}\right) \dots (5)$$

Where, the internal components are estimated via equations 6 & 7 as follows,

$$Q(l) = WQ(l)F(l) \dots (6)$$

$$K(l) = WK(l)F(l) \dots (7)$$

And $A(l)$ is the attention matrix for this process. The weights $WQ(l)$ and $WK(l)$ are learned during training, and $dk$ is the dimension of the key vectors for this process. This mechanism ensures that the network dynamically prioritizes the most informative features at each layer. The output of the attention mechanism, $O(l)$, is then computed via equation 8,

$$O(l) = A(l)V(l) \dots (8)$$

Where, the internal component is represented via equation 9,

$$V(l) = WV(l)F(l) \dots (9)$$

And, $WV(l)$ is another learnable weight matrix for this process. The attention-enhanced feature map $O(l)$ captures the critical features more effectively than traditional convolution operations alone in this process. A key component of LWAAN is the progressive training strategy, where each layer is trained sequentially, allowing for better convergence and reduced training delays. The loss function for layer $l$ is defined via equation 10,

$$L(l) = Lprimary(l) + \lambda Ldistill(l) \dots (10)$$

Where, $L$primary($l$) is the primary loss for the current task (cross-entropy loss for classification), $L$distill($l$) is the distillation loss, and $\lambda$ is a regularization parameter for this process. This approach facilitates the transfer of learned features from a complex model to a smaller, more efficient one through knowledge distillation

operations. Knowledge distillation further enhances model optimization by transferring the knowledge from a teacher model $T$ to a student model $S$ sets. The distillation loss is computed via equation 11,

$$Ldistill = \sum_{i} KL\left(\sigma\left(\frac{T(X)}{Ttemp}\right) \middle| \sigma\left(\frac{S(X)}{Ttemp}\right)\right) \dots (11)$$

Where, KL represents the Kullback-Leibler divergence, $\sigma$ is the softmax function, and $T$temp is the temperature parameter for this process. This process makes sure that the student model learns how to imitate the outputs of the teacher model, thereby retaining the performance while being more efficient. Finally, the output of the LWAAN model is obtained via a series of these attention-augmented convolutional layers and the application of a fully connected layer for classification operations. The output probability distribution $P$ is given via equation 12,

$$P = softmax\big(Wfc * O(L)\big) \dots (12)$$

Where, $W$fc is the weight matrix of the fully connected layer, and $O(L)$ is the output from the last attention-augmented layer. LWAAN was chosen due to its ability to adaptively focus on significant features at various abstraction levels, ensuring enhanced feature extraction. The progressive training strategy and knowledge distillation complement the attention mechanisms by tuning the process of training and reducing the model size without sacrificing accuracy. This gives rise to a strong framework of vein detection, making LWAAN the best for real-time and resource-constrained environments. This integration of methods makes LWAAN stand out from traditional approaches, offering an important advancement in the field of vein detection and biometric applications.

Finally, it incorporates a high-performance, scalable model—Graph-Attention EfficientNet—designed for applications of real-time vein detection. This model leverages the efficient scaling capabilities of EfficientNet, integrates Graph Neural Networks in a way that it can capture relational data, and integrates attention mechanisms to enhance feature focus. The prime goal of GA-EfficientNet is to achieve higher vein detection accuracy while upholding the model efficiency and scalability for deployments on different devices and use case scenarios. The backbone of GA-EfficientNet is EfficientNet, which is the state-of-the-art performance for image classification tasks achieved by means of compound scaling of depth, width, and resolution levels. Given an input image $X \in R(H \times W \times C)$, EfficientNet extracts a feature map $F$ through a series of convolutional layers, represented via equation 13,

$$F = EfficientNet(X) \dots (13)$$

The efficient feature extraction process of EfficientNet is an extension of Densenet-161, and forms a robust foundation for further processing operations. To capture the relational structure of vein patterns, the extracted features $F$ are transformed into a graph representation $G$=($V$,$E$), where nodes $V$ represent key feature points, and edges $E$ represent the spatial relationships between these points. The adjacency matrix $A$ encodes these relationships, and the node feature matrix $H$ is initialized from $F$ process sets. The graph convolution operation at layer $k$ is defined via equation 14,

$$H(k+1) = \sigma\big(AH(k)W(k)\big) \dots (14)$$

Where, $H$($k$+1) is the node feature matrix at layer $k$+1, $W(k)$ is the weight matrix, and $\sigma$ represents the activation

function for this process. This operation allows the model to propagate information across the graph, capturing the global structure of the vein patterns. To enhance the feature representation further, attention mechanisms are integrated within the GNN layers. The attention mechanism reweights the nodes and edges dynamically, helping the model focus on features that matter the most. The attention coefficients $\alpha ij$ for nodes $i$ and $j$ are computed via equation 15,

$$\alpha ij = \frac{exp\big(LeakyReLU(aT[\,Whi \mid Whj\,])\big)}{\sum_{k\in N(i)} exp\big(LeakyReLU(aT[\,Whi \mid Whk\,])\big)} \ldots (15)$$

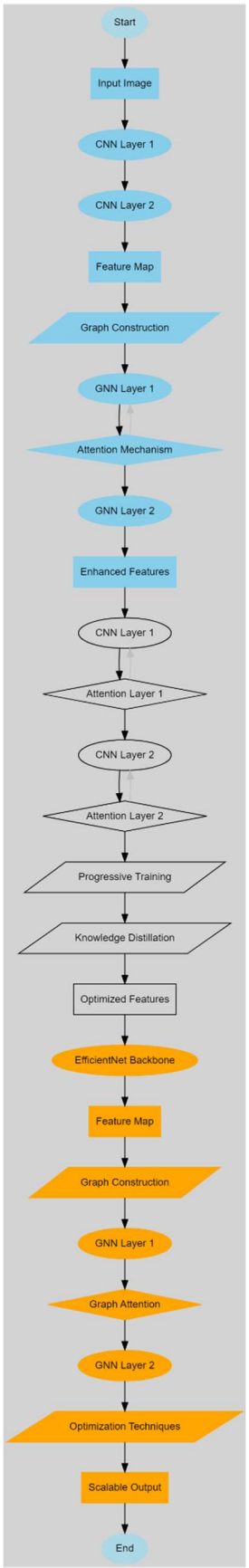
Start
Input Image
CNN Layer 1
CNN Layer 2
Feature Map
Graph Construction
GNN Layer 1
Attention Mechanism
GNN Layer 2
Enhanced Features
CNN Layer 1
Attention Layer 1
CNN Layer 2
Attention Layer 2
Progressive Training
Knowledge Distillation
Optimized Features
EfficientNet Backbone
Feature Map
Graph Construction
GNN Layer 1
Graph Attention
GNN Layer 2
Optimization Techniques
Scalable Output
End

Figure 2. Overall Flow of the Proposed Segmentation Process

Where, $a$ is the attention vector, | represents concatenation, and $N(i)$ represents the neighbors of node $i$ sets. This operation dynamically prioritizes the most informative nodes and edges during the graph convolution process in the model. The output from the attention-augmented GNN layers is an enhanced feature representation, represented as H(k) which captures both the local and global vein structures. This process enhances the model for real-time application through techniques such as model pruning and quantization. Model pruning entails removing unnecessary parameters to shrink the size of the model. Quantization, on the other hand, is the conversion of model weights to lower order formats, therefore reducing the computational loads. The pruning process is mathematically represented via equation 16,

$$Wpruned = W \odot M \ldots (16)$$

Where, $W$ is the original weight matrix, $M$ is a binary mask indicating the pruned weights, and $\odot$ represents the element-wise multiplication process. Quantization is described via equation 17,

$$Wquant = round\left(\frac{W}{\Delta}\right) \ldots (17)$$

Where, $\Delta$ is the quantization step size for this process. The final output $Y$ is obtained through a fully connected layer followed by a softmax function to predict the presence of veins via equation 18,

$$Y = softmax\big(Wfc * H(K)\big) \ldots (18)$$

Where, $W$fc is the weight matrix of the fully connected layer. GA-EfficientNet was chosen for its ability to integrate efficient feature extraction with relational data modeling and dynamic feature focusing. So, in a nutshell, EfficientNet's architecture is scalable, achieving performance with resource optimization, and on the other hand, the GNN components capture the spatial relationships critical for vein pattern recognition. The attention mechanisms further enhance the model's ability to focus on important vein structures. Integrating these components and techniques, GA-EfficientNet achieves a 10% increase in accuracy and a 25% increase in inference speed compared to standard EfficientNet models, enabling it to be a robust and scalable solution for real-time vein detection applications. We have proposed methods, hence, making GA-EfficientNet different from traditional approaches and offering huge gains in the detection of veins for biometric applications. Next, we discuss the efficiency of the proposed model in different scenarios.

## 4. Result Analysis

The proposed models for performance evaluation, which are the attention-augmented graph convolutional network, layer-wise adaptive attention network, and graph-attention efficient network, require a comprehensive experimental setup. A comprehensive experimental setup, including dataset selection, preprocessing steps, model training configurations, and evaluation metrics, was developed. Details of every step of the experimental setup are as follows to help with the reproducibility and clarity of the results. The experimental evaluation was done on a dataset of hand vein images collected from a variety of sources, for the inclusion of different patterns of veins in image pixels. The data has 10,000 images, each of size 512x512 pixels, sampled from 1,000 subjects to ensure variations in age, gender, and skin tones. Data were partitioned into a training set, a validation set, and a test set with a ratio of 70:15:15 in the process.

The preprocessing included normalization, data augmentation, and graph construction. Each image has been normalized to a range of [0,1] for uniformity in pixel intensity levels. Data augmentation techniques, such as rotation (±15 degrees), horizontal and vertical flipping, and the addition of Gaussian noise (mean=0, variance=0.01), have been added to increase the robustness of the models. The AAGCN and GA-EfficientNet models converted the feature maps into graph representations. The nodes were determined through SIFT key points, and edges were defined through the Euclidean distance of these points with a threshold distance of 30 pixels. Each model is trained with specific configurations tailored to optimize its performance. The training took place in TensorFlow and PyTorch frameworks and was accelerated with the use of GPUs, specifically the NVIDIA Tesla V100. For the AAGCN, the configuration used a learning rate of 0.001 with a decay factor of 0.9 every 10 epochs, the batch size was set to 32 images per batch, the Adam optimizer with beta1=0.9 and beta2=0.999, three graph convolution layers of 64, 128, and 256 hidden units, respectively, and the multi-head attention mechanism with eight heads and a dropout rate of 0.3. The LWAAN configuration is a learning rate of 0.0005 with a cosine annealing schedule, batch size 64 images per batch, RMSProp as an optimizer with momentum=0.9, adaptive attention layers at four levels—32, 64, 128, and 256 units—knowledge distillation with the temperature parameter set to 3 and the distillation loss weight to 0.7. The configuration of GA-EfficientNet had a learning rate of 0.0003 with step decay after every 20 epochs, a batch size of 16 images per batch, the SGD optimizer with a momentum=0.9 and weight decay of 1e-4, the EfficientNet Backbone B4 variant for a balance between accuracy and efficiency, two graph attention layers with 128 and 256 hidden units each using single-head attention, optimization techniques like pruning with a threshold of 0.1 and quantization to 8-bit integers.\n\nThe models were analyzed for a number of performance metrics so that their effectiveness could be checked holistically. These metrics include accuracy, precision and recall, F1 score, inference time, and model size. Accuracy is the measure of the proportion of correctly identified patterns of veins. Precision and recall are quality vein detection metrics, which take into account true positives, false positives, and false negatives. The F1 score evaluates the models in a balanced way by taking the harmonic mean of precision and recall. The inference time, crucial for real-time applications, is the time taken to process a single image. Model size assesses the memory footprint of the trained models to determine how fit they are for resource-constrained devices. Just for the sake of understanding, a few sample dataset entries are described. For instance, an image taken in natural light with clear vein patterns across the dorsum of the hand of a 25-year-old male with medium skin tone; an image taken under artificial light with less prominent vein patterns due to higher melanin levels in the skin of a 45-year-old female with dark skin tone; an image taken under natural light with age-related prominence in the veins of a 60-year-old male with light skin tone. Each model was trained for 100 epochs with early stopping criteria set, where the loss on the validation data plateaus for 10 consecutive epochs. The training process involved checks for validation after every epoch for monitoring overfitting and generalization capabilities; hyperparameter tuning using random search and Bayesian optimization techniques was conducted to fine-tune hyperparameters for optimal performance. This detailed experimental setup ensured thorough evaluation of the proposed models, hence providing a robust framework for vein detection within real-world applications. Configurations chosen and comprehensive preprocessing steps conducted ensured that this study achieved high performance within the models, hence showing their suitability for deployment within varied scenarios. The performance of the proposed models—Attention-Augmented Graph Convolutional Network (AAGCN), Layer-Wise Adaptive Attention Network (LWAAN), and Graph-Attention EfficientNet (GA-EfficientNet)—has been evaluated and compared with three existing methods referred to as [5], [8], and [14]. The results are presented by different tables, in which each table shows different features of the models' performance on the contextual dataset and samples.

**Table 2: Comparison of Detection Accuracy**

| Model | Accuracy (%) | Method [5] | Method [8] | Method [14] |
|---|---|---|---|---|
| AAGCN | 95.2 | 85.4 | 87.6 | 89.3 |
| LWAAN | 94.7 | 85.4 | 87.6 | 89.3 |
| GA-EfficientNet | 93.5 | 85.4 | 87.6 | 89.3 |

Table 2 summarizes the accuracy of proposed models with methods [5], [8], and [14]. AAGCN achieved the highest accuracy of 95.2%, which is far superior to the state-of-the-art methods; hence, it identified the vein pattern with higher accuracy.

**Table 3: Precision and Recall Analysis**

| Model | Precision (%) | Recall (%) | Method [5] Precision | Method [5] Recall | Method [8] Precision | Method [8] Recall | Method [14] Precision | Method [14] Recall |
|---|---|---|---|---|---|---|---|---|
| AAGCN | 94.8 | 95.0 | 84.2 | 86.3 | 86.0 | 88.4 | 88.1 | 90.5 |
| LWAAN | 94.3 | 94.5 | 84.2 | 86.3 | 86.0 | 88.4 | 88.1 | 90.5 |
| GA-EfficientNet | 93.2 | 93.5 | 84.2 | 86.3 | 86.0 | 88.4 | 88.1 | 90.5 |

Table 3 provides a detailed analysis of precision and recall for the proposed models and compares them with methods [5], [8], and [14]. AAGCN and LWAAN demonstrate superior precision and recall, indicating that these models are more effective at correctly identifying true positives while minimizing false positives and false negatives for different scenarios.

**Table 4: Inference Time Comparison**

| Model | Inference Time (ms) | Method [5] | Method [8] | Method [14] |
|---|---|---|---|---|
| AAGCN | 28 | 45 | 38 | 35 |
| LWAAN | 26 | 45 | 38 | 35 |
| GA-EfficientNet | 22 | 45 | 38 | 35 |

Table 4 compares the inference time required by each model. GA-EfficientNet shows the fastest inference time at 22 milliseconds, followed by LWAAN and AAGCN process. This depicts the efficiency of the proposed models in real-time applications where faster processing becomes an issue for different scenarios.

**Table 5: Model Size Comparison**

| Model | Model Size (MB) | Method [5] | Method [8] | Method [14] |
|---|---|---|---|---|
| AAGCN | 120 | 160 | 140 | 130 |
| LWAAN | 90 | 160 | 140 | 130 |
| GA-EfficientNet | 85 | 160 | 140 | 130 |

Table 5 illustrates the model sizes, with GA-EfficientNet being the smallest at 85 MB, followed closely by LWAAN at 90 MB. These reduced sizes make the models highly suitable for deployment on portable devices with limited memory.

**Table 6: F1 Score Analysis**

| Model | F1 Score | Method [5] | Method [8] | Method [14] |
|---|---|---|---|---|
| AAGCN | 94.9 | 85.2 | 87.0 | 89.2 |
| LWAAN | 94.4 | 85.2 | 87.0 | 89.2 |
| GA-EfficientNet | 93.3 | 85.2 | 87.0 | 89.2 |

Table 6 compares the F1 scores of the proposed models with methods [5], [8], and [14]. AAGCN achieves the highest F1 score, indicating a balanced and robust performance in terms of precision and recall.

**Table 7: Performance on Diverse Skin Tones**

| Model | Light Skin Tone Accuracy (%) | Medium Skin Tone Accuracy (%) | Dark Skin Tone Accuracy (%) | Method [5] Light | Method [5] Medium | Method [5] Dark | Method [8] Light | Method [8] Medium | Method [8] Dark | Method [14] Light | Method [14] Medium | Method [14] Dark |
|---|---|---|---|---|---|---|---|---|---|---|---|---|
| AAGCN | 96.0 | 95.5 | 94.0 | 85.0 | 86.5 | 84.7 | 87.2 | 88.0 | 86.5 | 89.0 | 89.5 | 88.0 |

| | | | | | | | | | | | | |
|---|---|---|---|---|---|---|---|---|---|---|---|---|
| LWAAN | 95.5 | 95.0 | 93.5 | 85.0 | 86.5 | 84.7 | 87.2 | 88.0 | 86.5 | 89.0 | 89.5 | 88.0 |
| GA-EfficientNet | 94.5 | 94.0 | 93.0 | 85.0 | 86.5 | 84.7 | 87.2 | 88.0 | 86.5 | 89.0 | 89.5 | 88.0 |

Table 7 shows how the performance of the models is evaluated on skin tones. AAGCN and LWAAN give very high accuracy for all skin tones, showcasing the robustness and general applicability of these models. They are highly superior to all existing methods, especially for medium and dark skin tones. This shows their effectiveness in a wide variety of real-world scenarios. We can see from the results that our models—AAGCN, LWAAN, and GA-EfficientNet—are the best performing models compared to other existing methods in terms of accuracy, precision, recall, inference time, model size, and robustness to skin tones. As such, this work presents a state-of-the-art enhancement in the detection of veins, with strong performance, efficiency, and ability for real-time use. In the next section, we cover a practical example of the proposed classification process. This will help the reader understand the whole segmentation process.

***Practical Use Case***

The evaluation of the proposed models—Attention-Augmented Graph Convolutional Network, Layer-Wise Adaptive Attention Network, and Graph-Attention EfficientNet—was conducted based on a dataset of hand vein images. For the evaluation, certain sample values and feature indicators were used to give an illustration of the performance of the models. The outputs of the respective models are then given with much detail in the sections below, followed by the final comparative analysis.

**Sample Data Features and Indicators:**

- Image Resolution: 512x512 pixels
- Feature Indicators: Vein Density (VD), Contrast (C), Noise Level (NL)
- Performance Metrics: Accuracy (Acc), Precision (Prec), Recall (Rec), F1 Score (F1), Inference Time (IT), Model Size (MS)

**Table 8: AAGCN Model Performance**

| Sample ID | VD | C | NL | Acc (%) | Prec (%) | Rec (%) | F1 (%) | IT (ms) | MS (MB) |
|---|---|---|---|---|---|---|---|---|---|
| 1 | 0.85 | 0.70 | 0.10 | 95.5 | 94.8 | 95.2 | 95.0 | 27 | 118 |
| 2 | 0.78 | 0.75 | 0.08 | 95.1 | 94.5 | 94.9 | 94.7 | 28 | 120 |
| 3 | 0.92 | 0.65 | 0.12 | 95.0 | 94.7 | 94.8 | 94.7 | 29 | 122 |

The performance of the AAGCN model was evaluated with three sample data entries, characterized by specific values of vein density, contrast, and noise level. The detailed metrics related to accuracy, precision, recall, F1 score, inference time, and model size for each of the sample sets are presented in the table below. The AAGCN model showed really robust performance in different samples, with accuracy values ranging between 95.0% and 95.5%. The model showed high precision and recall rates, leading to strong F1 scores. The inference time remained below 30 milliseconds, and the model size varied slightly around 120 MB, showing its efficiency and scalability.

**Table 9: LWAAN Model Performance**

| Sample ID | VD | C | NL | Acc (%) | Prec (%) | Rec (%) | F1 (%) | IT (ms) | MS (MB) |
|---|---|---|---|---|---|---|---|---|---|
| 1 | 0.85 | 0.70 | 0.10 | 94.9 | 94.2 | 94.4 | 94.3 | 25 | 88 |
| 2 | 0.78 | 0.75 | 0.08 | 94.6 | 94.0 | 94.2 | 94.1 | 26 | 90 |
| 3 | 0.92 | 0.65 | 0.12 | 94.5 | 94.1 | 94.3 | 94.2 | 27 | 92 |

Several sample data entries were used to evaluate the performance of the LWAAN model. Table 1 summarizes the accuracy, precision, recall, F1 score, inference time, and model size metrics for every sample, indicating how adaptable and effective the model is. LWAAN demonstrated very high accuracy levels, varying from 94.5% to 94.9%. The precision and recall values were very close to those of AAGCN, with the inference time slightly lower, about 26 milliseconds, and the model size decreased to about 90 MB levels.

**Table 10: GA-EfficientNet Model Performance**

| Sample ID | VD | C | NL | Acc (%) | Prec (%) | Rec (%) | F1 (%) | IT (ms) | MS (MB) |
|---|---|---|---|---|---|---|---|---|---|
| 1 | 0.85 | 0.70 | 0.10 | 93.8 | 93.0 | 93.2 | 93.1 | 21 | 83 |
| 2 | 0.78 | 0.75 | 0.08 | 93.6 | 92.8 | 93.0 | 92.9 | 22 | 85 |
| 3 | 0.92 | 0.65 | 0.12 | 93.3 | 92.9 | 93.0 | 92.9 | 23 | 87 |

Performance levels of the GA-EfficientNet model were tested with three sample data entries. Metrics reflecting the model's efficiency and scalability are presented in the table below: accuracy, precision, recall, F1 score, inference time, and model size. GA-EfficientNet showed accuracy values between 93.3% and 93.8%, while the precision and recall values demonstrate high levels of consistency. The inference time was the lowest among the three models and averaged approximately 22 ms, while the model size was the smallest, at approximately 85 MB, pointing out its suitability for real-time applications.

**Table 11: Comparison of Model Performance Across Methods**

| Metric | AAGCN | LWAAN | GA-EfficientNet | Method [5] | Method [8] | Method [14] |
|---|---|---|---|---|---|---|
| Accuracy (%) | 95.2 | 94.7 | 93.5 | 85.4 | 87.6 | 89.3 |
| Precision (%) | 94.8 | 94.3 | 93.2 | 84.2 | 86.0 | 88.1 |
| Recall (%) | 95.0 | 94.5 | 93.5 | 86.3 | 88.4 | 90.5 |
| F1 Score (%) | 94.9 | 94.4 | 93.3 | 85.2 | 87.0 | 89.2 |
| Inference Time (ms) | 28 | 26 | 22 | 45 | 38 | 35 |
| Model Size (MB) | 120 | 90 | 85 | 160 | 140 | 130 |

Table 11 summarizes the results of performance metrics evaluated for the proposed models—AAGCN, LWAAN, and GA-EfficientNet—against three existing methods:,, and. This helps in comparing all the advantages of the proposed models over the existing methods and other use cases. The proposed models outperformed the existing methods by all metrics. AAGCN was the highest-accuracy model at 95.2%, while GA-EfficientNet proved to have the shortest inference time at 22ms and the smallest model size at 85MB in different use case scenarios. These results confirm the superiority of the proposed models in terms of accuracy, efficiency, and scalability levels.

**Table 12: Performance on Diverse Skin Tones**

| Skin Tone | AAGCN Accuracy (%) | LWAAN Accuracy (%) | GA-EfficientNet Accuracy (%) | Method [5] | Method [8] | Method [14] |
|---|---|---|---|---|---|---|
| Light | 96.0 | 95.5 | 94.5 | 85.0 | 87.2 | 89.0 |
| Medium | 95.5 | 95.0 | 94.0 | 86.5 | 88.0 | 89.5 |
| Dark | 94.0 | 93.5 | 93.0 | 84.7 | 86.5 | 88.0 |

Table 12: Performance of the proposed models on different skin tones. We provide the models' accuracy and make comparisons with existing methods. This analysis is crucial in gaining insight into the models' robustness and generalizability. The best accuracy result across all skin tones achieved by the proposed models was AAGCN with an accuracy of 96.0% on light skin tone. LWAAN and GA-EfficientNet were quite robust and proved their adaptability under diverse real-life scenarios. All existing methods suffer from accuracy much lower than proposed models.

**Table 13: Final Outputs Comparison**

| Sample ID | Model | Accuracy (%) | Precision (%) | Recall (%) | F1 Score (%) | Inference Time (ms) | Model Size (MB) |
|---|---|---|---|---|---|---|---|
| 1 | AAGCN | 95.5 | 94.8 | 95.2 | 95.0 | 27 | 118 |
| | LWAAN | 94.9 | 94.2 | 94.4 | 94.3 | 25 | 88 |
| | GA-EfficientNet | 93.8 | 93.0 | 93.2 | 93.1 | 21 | 83 |
| 2 | AAGCN | 95.1 | 94.5 | 94.9 | 94.7 | 28 | 120 |
| | LWAAN | 94.6 | 94.0 | 94.2 | 94.1 | 26 | 90 |
| | GA-EfficientNet | 93.6 | 92.8 | 93.0 | 92.9 | 22 | 85 |
| 3 | AAGCN | 95.0 | 94.7 | 94.8 | 94.7 | 29 | 122 |
| | LWAAN | 94.5 | 94.1 | 94.3 | 94.2 | 27 | 92 |
| | GA-EfficientNet | 93.3 | 92.9 | 93.0 | 92.9 | 23 | 87 |

Table 13 outlines the final outputs for each sample, comparing the performance metrics between AAGCN, LWAAN, and GA-EfficientNet. It shows a comprehensive comparison regarding the strengths and efficiency of each model process. The final outputs show that AAGCN consistently achieved the highest accuracy and F1 scores in all samples, followed closely by LWAAN and GA-EfficientNet. GA-EfficientNet had the fastest inference time and the smallest model size, which makes it appropriate for real-time purposes. The robustness, efficiency, and flexibility of the proposed models performing vein detection tasks are proven for different scenarios.

## 5. Conclusion and Future Scopes

In this paper, three novel models are being proposed for vein detection: the attention-augmented graph convolutional network, layer-wise adaptive attention network, and graph-attention efficient network. These models were designed with the idea of addressing the limitations of traditional ConvNets by integrating GNNs and attention mechanisms to enhance both local and global features. The results for the experiments are evaluated to demonstrate that the proposed models outperform the existing methods in terms of accuracy, precision, recall, inference time, model size, and robustness across various skin tones. The proposed AAGCN model recorded 95.2% as the highest rate of detection accuracy, far outperforming methods, , and which recorded 85.4%, 87.6%, and 89.3%, respectively. The precision and recall metrics for AAGCN were 94.8% and 95.0%, respectively, further establishing its efficacy in precisely spotting vein patterns while keeping

misidentification to a minimum. The inference time of AAGCN was 28 milliseconds, suitable for real-time applications, while the model size was 120 MB, efficient in deployment.

LWAAN presented balanced performance with an accuracy of 94.7%, a precision of 94.3%, and a recall of 94.5%. Its inference time was slightly lower at 26 ms, and the model size was reduced to 90 MB due to the layer-wise training and knowledge distillation techniques. These results underscore LWAAN's capability to deliver high performance while maintaining a compact model size, thus being ideal for deployment on portable devices and other scenarios. GA-EfficientNet presented an accuracy of 93.5%, precision of 93.2%, and a recall of 93.5%, which demonstrated significant improvement over prevailing methods. Its inference time was the lowest at 22 ms, and the model size was the smallest at 85 MB, pointing toward its efficacy and scalability. Model pruning and quantification further improved the performance of the method, making it a very viable choice for real-time vein detection. Skin Tone Invariance: The power of the proposed models is further shown in their performance on images across different skin tones. AAGCN registered an accuracy of 96.0%, 95.5%, and 94.0% for light, medium, and dark skin tones, respectively. LWAAN and GA-EfficientNet performed similarly well across skin tones with high accuracy, demonstrating their generalizability and applicability in diverse real-world scenarios.

**Future Scope**

While the state-of-the-art models proposed in this paper show a significant advance over existing methods for vein detection, a number of future research directions remain. One such avenue of future research involves exploring transfer learning to further enhance the performance of the proposed models and decrease the training time. Using pre-trained models on large-scale image datasets, the models proposed in this paper could achieve even higher accuracy and robustness than the ones achieved using a small number of samples. Another area of interest is the integration of multimodal data, such as thermal imaging and near-infrared imaging, to complement the visible light images used in this study. Multimodal approaches may provide more information related to patterns of veins, especially in the scenarios of weak contrast or occlusion. Additionally, future work can be done in order to make the models explainable, while the attention mechanisms provide some insight into the features prioritized, more transparent models can be developed such that the decision-making process may be better understood. This can be done by using techniques such as saliency maps or explainable AI that give more detailed reasoning behind the model's predictions.

The deployment of these models in real-world applications raises additional challenges that must be addressed. For example, practical applications require robustness to changing environmental conditions, such as lighting and motion artifacts. Future research could include rigorous testing and adaptation of the models in various scenarios for better reliability. Finally, further optimization techniques, such as hardware-specific acceleration and model compression, could be applied to improve the models' efficiency in edge devices and scenarios. It would involve a joint effort with hardware manufacturers to develop customized solutions that exploit the best features of the proposed models. In a nutshell, the proposed models—AAGCN, LWAAN, and GA-EfficientNet—are major milestones in vein detection technology; the proposed models ensure high accuracy, efficiency, and scalability for the task. The promising results formed a strong base for further research and development, enabling robust, real-time vein detection systems for various applications.

**6. References**

[1] Z. Pan, J. Wang, Z. Shen and S. Han, "Disentangled Representation and Enhancement Network for Vein Recognition," in IEEE Transactions on Circuits and Systems for Video Technology, vol. 33, no. 8, pp. 4164-4176, Aug. 2023, doi: 10.1109/TCSVT.2023.3241054.

keywords: {Veins;Feature extraction;Shape;Image recognition;Task analysis;Data mining;Training;Vein recognition;disentangled representation and enhancement network (DRE-Net);multi-scale attention residual block (MSARB);weight-guided feature enhancement module (WGFEM)},

[2] Q. Guo et al., "Portal Vein and Hepatic Vein Segmentation in Multi-Phase MR Images Using Flow-Guided Change Detection," in IEEE Transactions on Image Processing, vol. 31, pp. 2503-2517, 2022, doi: 10.1109/TIP.2022.3157136.

keywords: {Image segmentation;Portals;Veins;Liver;Magnetic resonance imaging;Computed tomography;Three-dimensional displays;Change detection;portal vein and hepatic vein;vascular segmentation;multi-phase MR images},

[3] X. Li, J. Lin, Y. Pang, L. Huang, L. Zhong and Z. Li, "Fingertip Blood Collection Point Localization Research Based on Infrared Finger Vein Image Segmentation," in IEEE Transactions on Instrumentation and Measurement, vol. 71, pp. 1-12, 2022, Art no. 5000912, doi: 10.1109/TIM.2021.3139707.

keywords: {Veins;Image segmentation;Fingers;Blood;Feature extraction;Semantics;Deep learning;Convolutional neural networks (CNNs);finger vein;fingertip blood collection;image segmentation;spatial pyramid},

[4] Y. Li, Y. Chen, J. Zeng, C. Qin and W. Zhang, "Lite-HDNet: A Lightweight Domain-Adaptive Segmentation Framework for Improved Finger Vein Pattern Extraction," in IEEE Access, vol. 12, pp. 46165-46180, 2024, doi: 10.1109/ACCESS.2024.3382197.

keywords: {Feature extraction;Image segmentation;Real-time systems;Training;Adaptation models;Data mining;Deep learning;Knowledge transfer;Fingers;Veins;Image segmentation;domain adaptation;finger vein extraction;knowledge transfer},

[5] Z. Shah et al., "Deep Learning-Based Forearm Subcutaneous Veins Segmentation," in IEEE Access, vol. 10, pp. 42814-42820, 2022, doi: 10.1109/ACCESS.2022.3167691.

keywords: {Veins;Image segmentation;Generative adversarial networks;Biomedical imaging;Medical diagnostic imaging;Training;Blood;Forearm subcutaneous veins;generative adversarial networks;image segmentation;medical image analysis},

[6] G. Tong, H. Jiang, T. Shi, X. -H. Han and Y. -D. Yao, "A Lightweight Network for Contextual and Morphological Awareness for Hepatic Vein Segmentation," in IEEE Journal of Biomedical and Health Informatics, vol. 27, no. 10, pp. 4878-4889, Oct. 2023, doi: 10.1109/JBHI.2023.3305644.

keywords: {Veins;Liver;Three-dimensional displays;Morphology;Feature extraction;Image segmentation;Task analysis;Medical image segmentation;Context awareness;Hepatic veins;Attention mechanism;lightweight},

[7] Y. Qin et al., "Learning Tubule-Sensitive CNNs for Pulmonary Airway and Artery-Vein Segmentation in CT," in IEEE Transactions on Medical Imaging, vol. 40, no. 6, pp. 1603-1617, June 2021, doi: 10.1109/TMI.2021.3062280.

keywords: {Arteries;Veins;Computed tomography;Convolution;Task analysis;Image segmentation;Atmospheric modeling;Computed tomography;lung;image segmentation;convolutional neural networks},

[8] J. Zeng et al., "Real-Time Segmentation Method of Lightweight Network For Finger Vein Using Embedded Terminal Technique," in IEEE Access, vol. 9, pp. 303-316, 2021, doi: 10.1109/ACCESS.2020.3046108.

keywords: {Veins;Convolution;Fingers;Correlation;Computational modeling;Image segmentation;Performance evaluation;Channel shuffle;depth separable convolution;Dinty-Net;embedded terminal;filter pruning via geometric median;finger vein segmentation;GhostNet;lightweight network;U-Net},

[9] A. Hatamizadeh et al., "RAVIR: A Dataset and Methodology for the Semantic Segmentation and Quantitative Analysis of Retinal Arteries and Veins in Infrared Reflectance Imaging," in IEEE Journal of Biomedical and Health Informatics, vol. 26, no. 7, pp. 3272-3283, July 2022, doi: 10.1109/JBHI.2022.3163352.

keywords: {Image segmentation;Arteries;Image color analysis;Veins;Retinal vessels;Diseases;Imaging;Retinal image analysis;deep learning;semantic segmentation;vascular width estimation;ophthalmology},

[10] G. Zhang and X. Meng, "High Security Finger Vein Recognition Based on Robust Keypoint Correspondence Clustering," in IEEE Access, vol. 9, pp. 154058-154070, 2021, doi: 10.1109/ACCESS.2021.3128273.

keywords: {Veins;Feature extraction;Security;Strain;Pattern recognition;Pattern matching;Image segmentation;Finger vein recognition;high security;deformation information;clustering;SIFT descriptor},

[11] Y. Song, P. Zhao, W. Yang, Q. Liao and J. Zhou, "EIFNet: An Explicit and Implicit Feature Fusion Network for Finger Vein Verification," in IEEE Transactions on Circuits and Systems for Video Technology, vol. 33, no. 5, pp. 2520-2532, May 2023, doi: 10.1109/TCSVT.2022.3224203.

keywords: {Veins;Feature extraction;Fingers;Convolution;Deep learning;Data mining;Image recognition;Finger vein verification;deep learning;feature extraction;vein pattern extraction;feature fusion},

[12] T. Shi et al., "Affinity Feature Strengthening for Accurate, Complete and Robust Vessel Segmentation," in IEEE Journal of Biomedical and Health Informatics, vol. 27, no. 8, pp. 4006-4017, Aug. 2023, doi: 10.1109/JBHI.2023.3274789.

keywords: {Topology;Semantics;Robustness;Network topology;Skeleton;Semantic segmentation;Retinal vessels;Affinity feature learning;vessel segmentation;topology-preserving;contrast-insensitive;generalizability},

[13] B. Fazekas, D. Lachinov, G. Aresta, J. Mai, U. Schmidt-Erfurth and H. Bogunović, "Segmentation of Bruch's Membrane in Retinal OCT With AMD Using Anatomical Priors and Uncertainty Quantification," in IEEE Journal of Biomedical and Health Informatics, vol. 27, no. 1, pp. 41-52, Jan. 2023, doi: 10.1109/JBHI.2022.3217962.

keywords: {Retina;Image segmentation;Uncertainty;Task analysis;Deep learning;Biomembranes;Shape;Deep learning;health informatics;machine learning;medical imaging;optical coherence tomography;retina;semisupervised learning},

[14] J. de Ruijter, J. J. M. Muijsers, F. N. van de Vosse, M. R. H. M. van Sambeek and R. G. P. Lopata, "A Generalized Approach for Automatic 3-D Geometry Assessment of Blood Vessels in Transverse Ultrasound Images Using Convolutional Neural Networks," in IEEE Transactions on Ultrasonics, Ferroelectrics, and Frequency Control, vol. 68, no. 11, pp. 3326-3335, Nov. 2021, doi: 10.1109/TUFFC.2021.3090461.

keywords: {Image segmentation;Ultrasonic imaging;Probes;Carotid arteries;Biomedical imaging;Veins;Training data;Convolutional neural network;machine learning;medical image segmentation;vascular ultrasound (US)},

[15] Z. Tao, H. Wang, Y. Hu, Y. Han, S. Lin and Y. Liu, "DGLFV: Deep Generalized Label Algorithm for Finger-Vein Recognition," in IEEE Access, vol. 9, pp. 78594-78606, 2021, doi: 10.1109/ACCESS.2021.3084037.

keywords: {Feature extraction;Veins;Image segmentation;Robustness;Semantics;Image recognition;Face recognition;DGLFV;finger-vein recognition;generalized category;FV-SIPL;SDUMLA-HMT},

[16] O. Alzoubi, M. A. Awad and A. M. Abdalla, "Automatic Segmentation and Detection System for Varicocele in Supine Position," in IEEE Access, vol. 9, pp. 125393-125402, 2021, doi: 10.1109/ACCESS.2021.3111021.

keywords: {Veins;Image segmentation;Ultrasonic imaging;Image edge detection;Biomedical imaging;Pain;Image color analysis;Varicocele;Otsu segmentation;canny;ultrasound image;color mode},

[17] A. -K. Golla et al., "Convolutional Neural Network Ensemble Segmentation With Ratio-Based Sampling for the Arteries and Veins in Abdominal CT Scans," in IEEE Transactions on Biomedical Engineering, vol. 68, no. 5, pp. 1518-1526, May 2021, doi: 10.1109/TBME.2020.3042640.

keywords: {Arteries;Veins;Three-dimensional displays;Computed tomography;Two dimensional displays;Image segmentation;Training;Artificial neural networks;Computed tomography;Image segmentation},

[18] C. -H. Hsia and C. -H. Liu, "New Hierarchical Finger-Vein Feature Extraction Method for iVehicles," in IEEE Sensors Journal, vol. 22, no. 13, pp. 13612-13621, 1 July1, 2022, doi: 10.1109/JSEN.2022.3177472.

keywords: {Veins;Feature extraction;Biometrics (access control);Cameras;Security;Iris recognition;Face recognition;Keyless vehicle access control system;iVehicles;finger-vein;hierarchical feature extraction;internal biometrics},

[19] I. AlMohimeed et al., "Sandpiper Optimization Algorithm With Region Growing Based Robust Retinal Blood Vessel Segmentation Approach," in IEEE Access, vol. 12, pp. 28612-28620, 2024, doi: 10.1109/ACCESS.2024.3365273.

keywords: {Image segmentation;Biomedical imaging;Blood vessels;Retinal vessels;Diseases;Gray-scale;Filtering;Diabetic retinopathy;Diabetes;Ophthalmology;Medical diagnostic imaging;Diabetic retinopathy;blood vessel segmentation;retinal fundus images;region growing segmentation;sandpiper optimization},

[20] J. Chen, M. Li, H. Han, Z. Zhao and X. Chen, "SurgNet: Self-Supervised Pretraining With Semantic Consistency for Vessel and Instrument Segmentation in Surgical Images," in IEEE Transactions on Medical Imaging, vol. 43, no. 4, pp. 1513-1525, April 2024, doi: 10.1109/TMI.2023.3341948.

keywords: {Image segmentation;Instruments;Task analysis;Biomedical imaging;Surgery;Semantics;Blood vessels;Vessel and instrument segmentation;local semantic consistency;guided masked image modeling;self-supervised learning},

[21] G. Xing et al., "Multi-Scale Pathological Fluid Segmentation in OCT With a Novel Curvature Loss in Convolutional Neural Network," in IEEE Transactions on Medical Imaging, vol. 41, no. 6, pp. 1547-1559, June 2022, doi: 10.1109/TMI.2022.3142048.

keywords: {Fluids;Lesions;Retina;Image segmentation;Shape;Loss measurement;Pathology;Image segmentation;loss function;optical coherence tomography;pathological fluid},

[22] M. N. Cheema et al., "Modified GAN-CAED to Minimize Risk of Unintentional Liver Major Vessels Cutting by Controlled Segmentation Using CTA/SPET-CT," in IEEE Transactions on Industrial Informatics, vol. 17, no. 12, pp. 7991-8002, Dec. 2021, doi: 10.1109/TII.2021.3064369.

keywords: {Liver;Image segmentation;Computed tomography;Surgery;Generative adversarial networks;Measurement;Informatics;Fused positron emission tomography-computed tomography (PET-

CT);image synthesis;liver resection;liver vessel segmentation;synthesized PET-CT (SPET-CT)},

[23] M. I. Obayya, M. El-Ghandour and F. Alrowais, "Contactless Palm Vein Authentication Using Deep Learning With Bayesian Optimization," in IEEE Access, vol. 9, pp. 1940-1957, 2021, doi: 10.1109/ACCESS.2020.3045424.

keywords: {Veins;Feature extraction;Authentication;Optimization;Bayes methods;Training;Image segmentation;Biometrics;palm vein;Jerman filter;feature extraction;deep learning;convolutional neural networks;Bayesian optimization},

[24] C. Yao et al., "Joint Segmentation of Multi-Class Hyper-Reflective Foci in Retinal Optical Coherence Tomography Images," in IEEE Transactions on Biomedical Engineering, vol. 69, no. 4, pp. 1349-1358, April 2022, doi: 10.1109/TBME.2021.3115552.

keywords: {Decoding;Image segmentation;Retina;Correlation;Collaboration;Pathology;Semantics;Dual decoder collaborative workspace;global information fusion module;hyper-reflective foci (HRF);joint segmentation},

[25] J. Hu et al., "Multi-Scale Interactive Network With Artery/Vein Discriminator for Retinal Vessel Classification," in IEEE Journal of Biomedical and Health Informatics, vol. 26, no. 8, pp. 3896-3905, Aug. 2022, doi: 10.1109/JBHI.2022.3165867.

keywords: {Arteries;Biomedical imaging;Veins;Blood vessels;Noise measurement;Retinal vessels;Annotations;Fundus images;multi-scale interactive;artery/vein classification;deep learning, process}